第 49 卷 第 8 期/2022 年 4 月/中国激光 研究论文

中国激光

激光沉积制备 316L-IN625 梯度材料的组织与力学性能

余满江[1]，吴成萌[1]，冯爱新[1,2*]，张成龙[1]，徐国秀[1]

[1]温州大学机电工程学院，浙江 温州 325035；

[2]浙江省激光加工机器人重点实验室，浙江 温州 325035

摘要 采用激光沉积工艺制备了材料成分呈梯度变化的 316L-IN625 梯度材料，通过扫描电镜观察、X 射线衍射、拉伸测试等分析技术研究了梯度材料不同区域的显微组织形态，以及连接试样、梯度试样的力学性能。结果表明：梯度材料不同区域的显微组织随着 316L 成分的减少依次呈现为胞状枝晶、柱状晶、粗糙枝晶与近等轴晶；与连接试样相比，316L-IN625 梯度试样的屈服强度($\sigma_{0.2}$)升高至 289 MPa，但由于高的热应力与脆性析出相的存在，其抗拉强度与延展性均有所降低；脆性析出相随着拉伸应力的增大发生不均匀的塑性变形，导致梯度试样发生脆性解离。IN625 合金的固溶强化与析出强化，使得 316L-IN625 梯度材料的显微硬度沿沉积建造方向逐渐升高。

关键词 激光技术；激光沉积；316L-IN625 梯度材料；微观组织；力学性能

中图分类号 TG142.1 **文献标志码** A **doi**：10.3788/CJL202249.0802007

1 引 言

在制造核能发电设施的换热管与压力容器[1]中，常见由铁素体钢与奥氏体合金组成的异种金属接头。然而，这种接头两端材料的热膨胀系数以及弹性模量不匹配，巨大的温差使得接头内部产生了高的热应力，导致其性能下降。为此，研究人员试图将镍基高温合金填充至接头处，以提高铁素体钢与奥氏体合金的连接强度[2-3]。尽管人们已证明该方法可减小热膨胀系数的不匹配程度，但接头处的显微组织突变，以及应力腐蚀开裂导致构件失效的问题仍然存在[4]。梯度材料的显微组织及性能依据材料成分的变化而逐层过渡或连续过渡[5-7]，其内部的应力变化更为平缓，有助于延长异种金属复合构件的服役寿命[8-10]。

激光沉积设备配备了多个粉末供给体系，因此其所沉积的涂层可以是不同的材料成分，非常适宜制备材料成分渐变的梯度材料[11-13]。近年来，关于激光沉积制备由奥氏体合金与镍基高温合金组成的梯度材料已得到了研究人员的广泛关注。Lin 等[14]采用激光快速成型技术成功制造了 SS316L-Rene88DT 梯度材料，并研究了显微组织在成分梯度区域的凝固行为与形态演变；Shah 等[15]研究了激光直接金属沉积成型的 SS316L-IN718 梯度材料，结果发现，当 IN718 的成分比例足够高时，生成的 MC 型碳化物(NbC)可以有效提高材料的硬度以及耐磨性。值得注意的是，在 SS316L-IN625 梯度材料的激光定向能量沉积制备过程中，材料成分的连续性渐变会在其内部产生未熔颗粒与裂纹等缺陷。先前的报道对于这些缺陷成因的解释主要包括两方面：1)梯度区域不同沉积层的热传导以及激光吸收率不均匀[16]；2)梯度区域内大量富 Nb 与富 Mo 相的析出[17]。正如 Bobbio 等[18]早期的主张，材料成分的连续性渐变对增材制造成型梯度材料并不是绝对有利的。Zhang 等[19]采用直接能量沉积技术制备了 316L-IN625 梯度材料，他们通过引入中间层(50% 316L+50% IN625，均为质量分数)使得显微组织在梯度界面处渐变，在成型的梯度材料内未观察到裂纹、未熔颗粒与孔隙等成型缺陷。因

收稿日期：2021-07-02；**修回日期**：2021-08-10；**录用日期**：2021-09-26

基金项目：温州市科技计划项目(2018ZG018)

通信作者：*aixfeng@wzu.edu.cn

此，合理地选择中间层材料的成分，在减小热膨胀系数不匹配的同时避免成型缺陷是激光沉积制备316L-IN625 梯度材料的关键。

在本次试验中，本课题组采用激光沉积工艺，通过沿沉积建造方向依次改变 316L 与 IN625 的成分比例，制备了材料成分梯度变化的 316L-IN625 梯度试样，研究了梯度试样不同区域的显微组织形态，以及连接试样、梯度试样的力学性能。

2 试验与表征方法

2.1 试验方法

采用真空感应气雾化制粉炉制备粒径为 45～105 μm 的 316L 不锈钢粉末与 IN625 合金粉末。图 1 为 316L 不锈钢粉末与 IN625 合金粉末的微观形貌，可以看出，粉末颗粒尺寸相对均匀，且主要为球形。表 1 为 316L 不锈钢粉末与 IN625 合金粉末的化学成分。

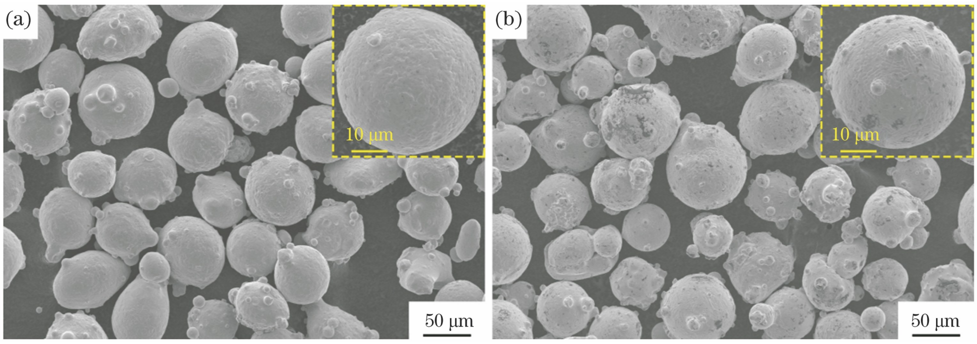

图 1 316L 不锈钢粉末与 IN625 合金粉末的微观形貌。(a) 316L；(b) IN625

Fig. 1 Micromorphologies of 316L stainless steel and IN625 alloy powders. (a) 316L; (b) IN625

表 1 316L 不锈钢粉末与 IN625 合金粉末的化学成分

Table 1 Chemical composition of 316L stainless steel and IN625 alloy powders

Powder	Mass fraction of element /%								
	Cr	Mo	Mn	Si	C	Nb	Al	Ni	Fe
316L	16.79	2.42	0.20	1.00	0.006			10.66	Bal.
IN625	21.28	8.54	0.049	0.19	0.040	3.55	0.019	Bal.	2.41

激光沉积试验在 LD-8060 送粉式金属 3D 打印设备上进行。该设备配备有 Laserline 公司的 LDF 6000-60 高功率半导体激光器、Precitec 公司的 YC52 同轴激光加工头（输出的高斯光束直径为 3 mm）、南京中科煜宸激光技术有限公司的 RC-PGF-D 双桶双控式送粉器以及西门子公司的数控系统。选用表面抛光的锻造 304L 不锈钢（尺寸为 105 mm×105 mm×20 mm）作为基板，保持总的粉末供给速度不变，通过沿沉积建造方向（BD）依次改变 316L 与 IN625 的成分比例来制备 316L-IN625 梯度试样，试样尺寸为 100 mm×15 mm×70 mm，如图2(a)所示。在激光沉积过程中，粉末颗粒经同

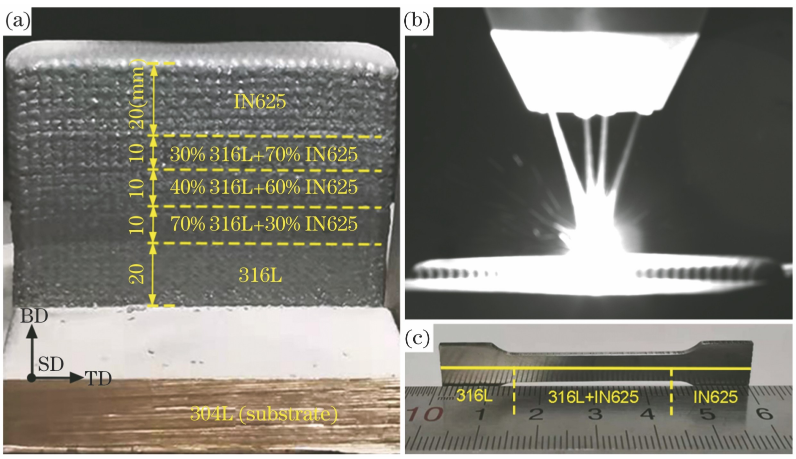

图 2 316L-IN625 梯度材料与拉伸试样的设计。(a)激光沉积制备的梯度试样；(b)同轴激光加工头；(c)梯度材料的拉伸试样

Fig. 2 Designs of gradient material and tensile specimens of 316L-IN625. (a) Gradient sample prepared by laser deposition; (b) coaxial laser processing head; (c) tensile specimen of gradient material

轴激光加工头的四路径向对称喷嘴[如图 2(b)所示]注入熔池，执行沿短边(SD)的蛇形扫描策略。同时，流速为 5 L/min 的同轴氩气吹向熔化表面，防止表面氧化。试验所选用的具体工艺参数如下：激光功率为 1300 W，扫描速度为 600 mm/min，粉末供给速度为 5.6 g/min，抬升量为 0.4 mm，搭接率为 50%。此外，制备 316L-IN625 连接试样(35 mm 316L+35 mm IN625，35 mm 为试样在 BD 方向的高度)，用于力学性能的对照研究。

2.2 表征方法

使用线切割机在 316L-IN625 梯度材料的不同区域截取金相试样，依据标准流程对金相试样的表面(平行于 SD 方向)进行研磨、抛光和腐蚀。腐蚀液为王水，由 HCl 与 HNO_3 按体积比为 3∶1配制而成。采用 BX53M 光学显微镜(OM)与 SU5000 扫描电子显微镜(SEM)对腐蚀后的微观组织进行观察；采用 Ultima IV 型 X 射线衍射仪(XRD)对不同区域的物相构成进行检测，并使用 MDI Jade 6.0 软件对晶面的半峰全宽进行计算。

沿平行于 SD 方向在 316L-IN625 梯度材料中部截取拉伸试样，截取的拉伸试样如图 2(c)所示。拉伸测试在 ZwickRoell 公司的 Z250 万能试验机上进行，拉伸速度为 3 mm/min；拉伸测试结束后，使用 SEM 对断口形貌进行观察；采用三丰株式会社的 HM-200 显微维氏硬度计，沿沉积建造方向对 316L-IN625 连接试样、梯度试样的显微硬度进行检测，试验力为 2.94 N，保压时间为 10 s。考虑到结果的可重复性，拉伸测试与显微硬度测试在相同的测试条件下各进行三次，并计算测试结果的平均值与标准偏差。

3 分析与讨论

3.1 316L-IN625 梯度材料的微观组织

图 3 为 316L-IN625 梯度材料不同区域的 OM 与 SEM 图，可以观察到沿着沉积建造方向，显微组织随着 316L 成分的减少依次呈现为胞状枝晶、柱状晶、粗糙枝晶与近等轴晶。316L 区域的晶界交汇处出现了微孔洞，孔洞内部存在形状不规则的夹杂物。在激光沉积过程中，熔池内部流体的流动随着 Benard-Marangoni 的不稳定而加剧[20]，导致晶界交汇处的成分偏析更加严重，因此产生了形状不规则的夹杂物。这种夹杂物与晶体之间的结合力很小，最终演变为微孔洞。Sun 等[21]在晶界处也发现了相似的夹杂物，并指出它们与增材制造过程中的氧化有关。此外，由图 3 还可以看出，70%316L 区域的胞状枝晶的晶界变宽，晶界处的微孔洞消失。随着沉积建造高度的增加，热累积效应使得冷却速率降低，Mo 充分扩散至晶界，晶界处高的溶质原子含量使晶界变宽并消除了晶界缺陷。

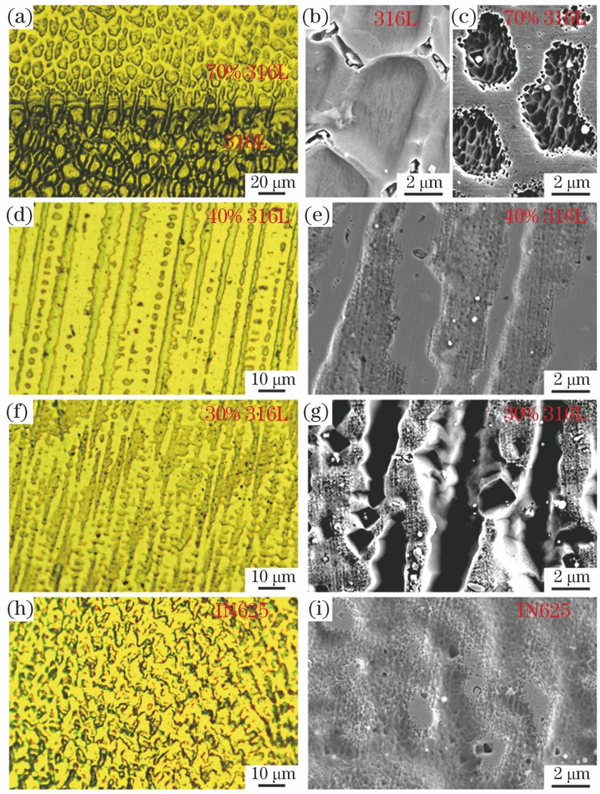

图 3 316L-IN625 梯度材料不同区域的 OM 与 SEM 图。(a)～(c) 316L 区域与 70% 316L 区域；(d)(e) 40% 316L 区域；(f)(g) 30% 316L 区域；(h)(i) IN625 区域

Fig. 3 OM and SEM images of different regions of 316L-IN625 gradient material. (a)-(c) 316L and 70% 316L regions; (d)(e) 40% 316L region; (f)(g) 30% 316L region; (h)(i) IN625 region

在 40% 316L 区域出现了外延生长的柱状晶。柱状晶的生长通常沿着温度梯度的方向并垂直于固液界面[22-23]。在 30% 316L 区域，显微组织向粗糙枝晶转变，一次枝晶间距减小(与 40% 316L 区域相比)。在相对较低的冷却速率下，熔池中晶体的成核速率小于其生长速率，从而促进了枝晶的生长；而一次枝晶间距的减小可能是由 Ni 含量升高(熔点升高)导致熔池过热度降低造成的。在 316L-IN625 梯度材料顶部(IN625 区域)，热累积的缓解使得冷却速率加快，枝晶的生长不再占据主导作用，因此生成了近等轴晶。

图 4 为 316L-IN625 梯度材料不同区域的 XRD 谱与(200)晶面的半峰全宽。从图4(a)可以看出，

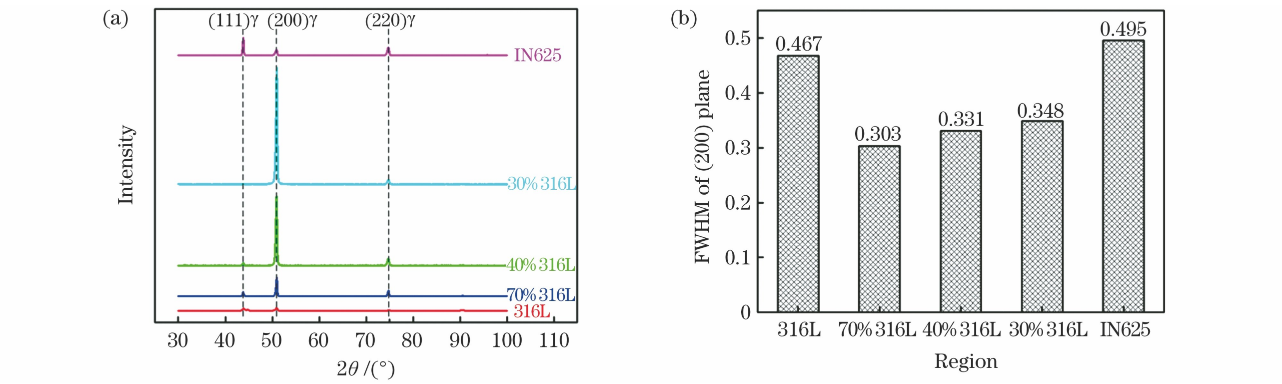

图 4 316L-IN625 梯度材料不同区域的 XRD 图谱与晶面的半峰全宽。(a)XRD 图谱;(b) (200)晶面的半峰全宽

Fig. 4 XRD spectra and crystal plane full width at half maximum (FWHM) of different regions of 316L-IN625 gradient material. (a) XRD spectra; (b) FWHM of (200) plane

不同区域仅存在多晶奥氏体结晶相。此外,梯度区域(70% 316L 区域、40% 316L 区域与 30% 316L 区域)的奥氏体择优沿(200)晶面方向生长,且具有相对较小的半峰全宽值,如图 4(b)所示。小的半峰全宽值反映了尖锐的衍射峰,说明在激光沉积过程中产生了高的热应力,从而导致了高的晶格畸变,这与 Zhong 等[24]的研究结果一致。

3.2 316L-IN625 梯度材料的力学性能

3.2.1 拉伸性能

316L-IN625 连接试样与梯度试样的拉伸性能如图 5 所示。从图 5 (a)可以看出,连接试样与梯度试样在屈服之前均发生了弹性变形,当塑性变形达到最大应力值时,试样断裂。由于连接试样产生了集中变形,其颈缩现象大于梯度试样。相比于连接试样,梯度试样的抗拉强度与延展性均有所降低,但其屈服强度有所升高,$\sigma_{0.2}$=289 MPa,如图 5 (b)所示。在拉伸测试中发现:连接试样的断裂发生在 316L 区域,其抗拉强度接近通过激光沉积制备的 316L 试样[19];梯度试样的断裂发生在 30% 316L 区域。由于梯度试样结合了 IN625 的高强度,因此其屈服强度有所升高。不过该区域所产生的高的热应力(见 3.1 节),以及可能存在的脆性析出相(Laves 相)[25],易使试样在拉伸测试的早期产生裂纹,导致其抗拉强度与延展性降低。

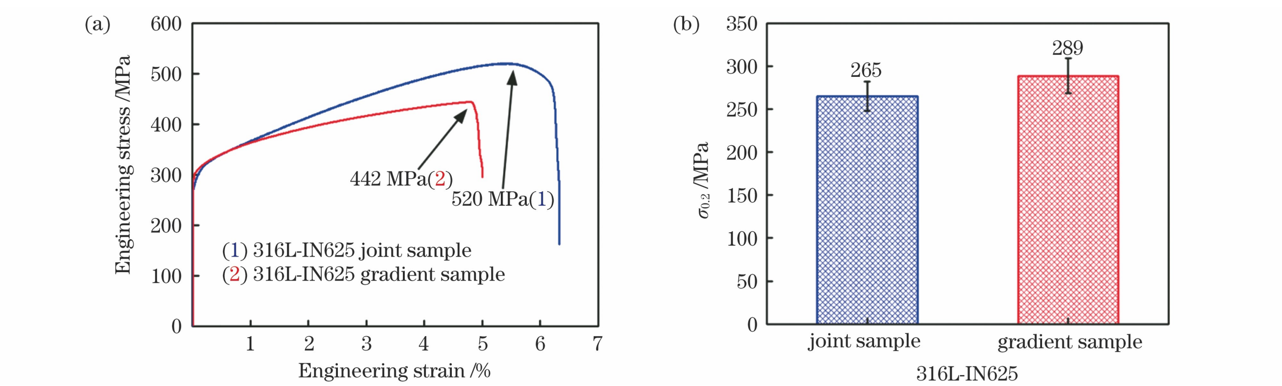

图 5 316L-IN625 连接试样与梯度试样的拉伸性能。(a)应力-应变曲线;(b)屈服强度($\sigma_{0.2}$)

Fig. 5 Tensile properties of joint and gradient samples of 316L-IN625. (a) Stress-strain curves; (b) yield strength ($\sigma_{0.2}$)

3.2.2 断口形貌

对断口形态的分析有助于进一步理解材料的变形机制。图 6 为 316L-IN625 连接试样与梯度试样的断口形貌,可以看出,断口上出现了不均匀分布的小孔,这些小孔通常在材料分离前产生,最终表现为延性破坏。对于连接试样,小孔出现在包含球形夹杂物的凹坑的底部。球形夹杂物在拉伸测试过程中更易实现均匀的塑性变形,因此产生了延性孔穴。然而,梯度试样中的小孔出现在包含析出相的凹坑的底部与顶部。与 316L 区域的变形机制不同,梯度试样的 30% 316L 区域产生的脆性析出相随着拉伸应力的增加与基体分离,之后由于不均匀塑性变形,试样发生脆性解离。因此,断口的整体形貌主要取决于孔核的分布以及小孔的逐步形核、扩展等过程。

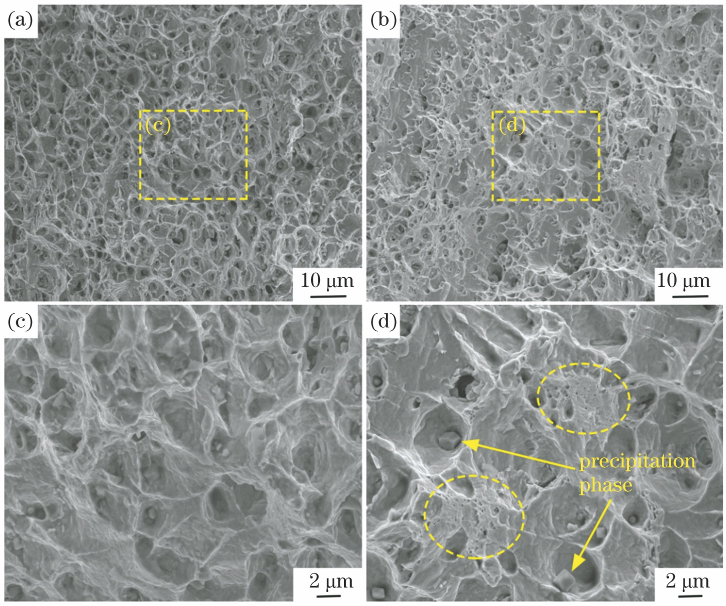

图 6 316L-IN625 连接试样与梯度试样的断口形貌。(a)(c)连接试样;(b)(d)梯度试样

Fig. 6 Fracture morphologies of joint and gradient samples of 316L-IN625. (a)(c) Joint sample; (b)(d) gradient sample

3.2.3 显微硬度

图 7 为 316L-IN625 连接试样与梯度试样的显微硬度分布。从图 7 可以看出,316L 区域的平均硬度为 174.7 HV,IN625 区域的平均硬度为 226.9 HV。

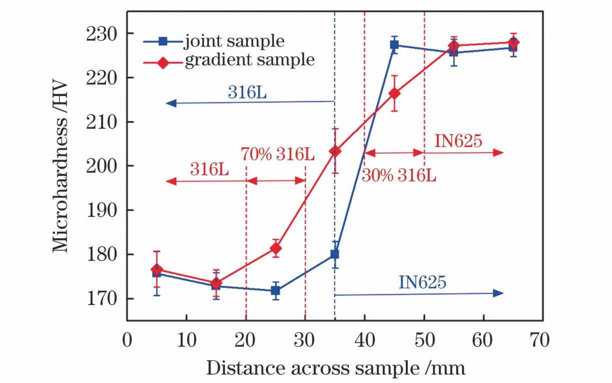

图 7 316L-IN625 连接试样与梯度试样的显微硬度分布

Fig. 7 Microhardness distribution of joint and gradient samples of 316L-IN625

对于连接试样,由于异种材料在接头处的显微组织突变,因此显微硬度急剧升高。然而,梯度试样中材料成分的梯度变化使得其显微硬度沿着沉积建造方向逐渐升高。与 316L 不锈钢相比,IN625 合金主要通过难溶金属(Nb 和 Mo)在冷却过程中保留在奥氏体基体的固溶体中实现固溶强化[26]。此外,对于 316L-IN625 梯度材料的激光沉积来说,位于先前沉积层中的 Nb、Mo 在持续的热循环条件下不断聚集,并最终以金属间相与碳化物的形式从基体中析出[27],实现析出强化。在 IN625 合金区域,固溶强化与析出强化的共同作用使得显微硬度达到最高值。

4 结　论

本研究采用激光沉积工艺,沿着沉积建造方向通过依次改变 316L 与 IN625 的成分比例来制备材料成分呈梯度变化的 316L-IN625 梯度材料。随着 316L 的减少,梯度材料不同区域的显微组织依次呈现为胞状枝晶、柱状晶、粗糙枝晶与近等轴晶。与连接试样相比,316L-IN625 梯度试样的屈服强度有所升高,为 289 MPa。此外,连接试样与梯度试样的拉伸变形机制分别为延性孔穴与脆性解离。316L-IN625 梯度材料的显微硬度沿着沉积建造方向逐渐升高,这与 IN625 自身所具有的固溶强化、析出强化有关。

参 考 文 献

[1] Zuback J S, Palmer T A, DebRoy T. Additive manufacturing of functionally graded transition joints between ferritic and austenitic alloys[J]. Journal of Alloys and Compounds, 2019, 770: 995-1003.

[2] DuPont J N. Microstructural evolution and high temperature failure of ferritic to austenitic dissimilar welds[J]. International Materials Reviews, 2012, 57(4): 208-234.

[3] Reichardt A, Shapiro A A, Otis R, et al. Advances in additive manufacturing of metal-based functionally graded materials [J]. International Materials Reviews, 2021, 66(1): 1-29.

[4] Yeh T K, Huang G R, Wang M Y, et al. Stress corrosion cracking in dissimilar metal welds with 304L stainless steel and alloy 82 in high temperature water[J]. Progress in Nuclear Energy, 2013, 63: 7-11.

[5] Liu Z Q, Meyers M A, Zhang Z F, et al. Functional gradients and heterogeneities in biological materials: design principles, functions, and bioinspired applications[J]. Progress in Materials Science, 2017, 88: 467-498.

[6] Sarathchandra D T, Subbu S K, Venkaiah N. Functionally graded materials and processing techniques: an art of review[J]. Materials Today: Proceedings, 2018, 5(10): 21328-21334.

[7] Li P F, Gong Y D, Zhou J Z, et al. Interface characteristics of abrupt gradient materials fabricated by laser cladding[J]. Laser & Optoelectronics Progress, 2021, 58(7): 0714011.
李鹏飞, 巩亚东, 周建忠, 等. 激光熔覆突变梯度材料界面特征研究[J]. 激光与光电子学进展, 2021, 58(7): 0714011.

[8] Larson E A, Ren X D, Adu-Gyamfi S, et al. Effects of scanning path gradient on the residual stress distribution and fatigue life of AA2024-T351 aluminium alloy induced by LSP[J]. Results in Physics, 2019, 13: 102123.

[9] Hu Y, Liu S S, Cheng X, et al. Finite element simulation on bending properties of TA2/TA15 gradient material by laser direct deposition[J]. Chinese Journal of Lasers, 2020, 47(12): 1202006.
胡悦, 刘莎莎, 程序, 等. 激光直接沉积 TA2/TA15 梯度材料弯曲性能的有限元模拟[J]. 中国激光, 2020, 47(12): 1202006.

[10] Gu D D, Zhang H M, Chen H Y, et al. Laser additive manufacturing of high-performance metallic aerospace components[J]. Chinese Journal of Lasers, 2020, 47(5): 0500002.
顾冬冬, 张红梅, 陈洪宇, 等. 航空航天高性能金属材料构件激光增材制造[J]. 中国激光, 2020, 47(5): 0500002.

[11] Yan L, Chen Y T, Liou F. Additive manufacturing of functionally graded metallic materials using laser metal deposition[J]. Additive Manufacturing, 2020, 31: 100901.

[12] Ji X, Sun Z G, Chang L L, et al. Microstructure evolution behavior in laser melting deposition of Ti6Al4V/Inconel625 gradient high-temperature resistant coating[J]. Chinese Journal of Lasers, 2019, 46(11): 1102008.
季霄, 孙中刚, 唱丽丽, 等. 激光熔化沉积 Ti6Al4V/Inconel625 梯度耐高温涂层组织演变行为研究[J]. 中国激光, 2019, 46(11): 1102008.

[13] Ansari M, Jabari E, Toyserkani E. Opportunities and challenges in additive manufacturing of functionally graded metallic materials via powder-fed laser directed energy deposition: a review[J]. Journal of Materials Processing Technology, 2021, 294: 117117.

[14] Lin X, Yue T M, Yang H O, et al. Laser rapid forming of SS316L/Rene88DT graded material[J]. Materials Science and Engineering A, 2005, 391(1/2): 325-336.

[15] Shah K, Haq I U, Khan A, et al. Parametric study of development of Inconel-steel functionally graded materials by laser direct metal deposition[J]. Materials & Design, 2014, 54: 531-538.

[16] Savitha U, Reddy G J, Venkataramana A, et al. Chemical analysis, structure and mechanical properties of discrete and compositionally graded SS316-IN625 dual materials[J]. Materials Science and Engineering A, 2015, 647: 344-352.

[17] Meng W, Zhang W H, Zhang W, et al. Fabrication of steel-Inconel functionally graded materials by laser melting deposition integrating with laser synchronous preheating[J]. Optics & Laser Technology, 2020, 131: 106451.

[18] Bobbio L D, Otis R A, Borgonia J P, et al. Additive manufacturing of a functionally graded material from Ti-6Al-4V to invar: experimental characterization and thermodynamic calculations[J]. Acta Materialia, 2017, 127: 133-142.

[19] Zhang X C, Chen Y T, Liou F. Fabrication of SS316L-IN625 functionally graded materials by powder-fed directed energy deposition[J]. Science and Technology of Welding and Joining, 2019, 24(5): 504-516.

[20] Casati R, Lemke J, Vedani M. Microstructure and fracture behavior of 316L austenitic stainless steel produced by selective laser melting[J]. Journal of Materials Science & Technology, 2016, 32(8): 738-744.

[21] Sun Y, Hebert R J, Aindow M. Non-metallic inclusions in 17-4PH stainless steel parts produced by selective laser melting[J]. Materials & Design, 2018, 140: 153-162.

[22] Zuback J S, Palmer T A, DebRoy T. Additive manufacturing of functionally graded transition joints between ferritic and austenitic alloys[J]. Journal of Alloys and Compounds, 2019, 770: 995-1003.

[23] Huang L F, Sun Y N, Ji Y Q, et al. Investigation of microstructures and mechanical properties of laser-melting-deposited $AlCoCrFeNi_{2.5}$ high entropy alloy[J]. Chinese Journal of Lasers, 2021, 48(6):

0602107.
黄留飞，孙耀宁，季亚奇，等. 激光熔化沉积 $AlCoCrFeNi_{2.5}$ 高熵合金的组织与力学性能研究[J]. 中国激光，2021，48(6)：0602107.

[24] Zhong Y, Rännar L E, Liu L F, et al. Additive manufacturing of 316L stainless steel by electron beam melting for nuclear fusion applications [J]. Journal of Nuclear Materials, 2017, 486: 234-245.

[25] Wang P, Zhang B C, Tan C C, et al. Microstructural characteristics and mechanical properties of carbon nanotube reinforced Inconel625 parts fabricated by selective laser melting [J]. Materials & Design, 2016, 112: 290-299.

[26] Marchese G, Colera X G, Calignano F, et al. Characterization and comparison of Inconel625 processed by selective laser melting and laser metal deposition [J]. Advanced Engineering Materials, 2017, 19(3): 1600635.

[27] Rombouts M, Maes G, Mertens M, et al. Laser metal deposition of Inconel625: microstructure and mechanical properties [J]. Journal of Laser Applications, 2012, 24(5): 052007.

Microstructure and Mechanical Properties of 316L-IN625 Gradient Material Prepared via Laser Deposition

Yu Manjiang[1], Wu Chengmeng[1], Feng Aixin[1,2*], Zhang Chenglong[1], Xu Guoxiu[1]

[1] *College of Mechanical & Electrical Engineering, Wenzhou University, Wenzhou, Zhejiang* 325035, *China*;

[2] *Key Laboratory of Laser Processing Robot of Zhejiang Province, Wenzhou, Zhejiang* 325035, *China*

Abstract

Objective Dissimilar metal joints composed of ferritic steel and austenitic alloy are widely used in the heat exchange tubes and pressure vessels of nuclear power generation facilities. However, there is a mismatch in the thermal expansion coefficients (CTE) of the materials at both ends of these joints. In addition, the high thermal stress inside the joints caused by a huge temperature gradient results in performance degradation. To reduce the CTE mismatch, the joints can be filled with nickel-based superalloys. Nonetheless, the problem of component failure due to mutations in the microstructure at the joints still exists. This problem can be resolved by a typical characteristic of the gradient materials, i. e., layer-by-layer or continuous change in their microstructure and performance with the changing material composition. Laser deposition (LD) is equipped with a flexible powder supply system, which makes it suitable for the preparation of gradient materials with gradual composition. However, this composition is not beneficial to gradient materials in all situations because gradient materials composed of 316L and IN625 still produce defects, such as unmelted particles and cracks, during the LD process. In view of this background, to select the optimal composition in the intermediate regions, 316L-IN625 gradient material was prepared by LD in this study. The microstructures of different regions of the gradient material and the mechanical properties, including joint and gradient samples, were studied. The results reveal the relationship between the microstructure and mechanical properties of the 316L-IN625 gradient material, and provide a reference for further study.

Methods The 316L stainless steel and IN625 alloy powders with a particle size of 45–105 μm were produced through vacuum atomization furnace (Fig. 1), and LD experiment was performed using the LD-8060 powder feeding metal 3D printing equipment. During the LD process, keeping the total powder supply rate unchanged, 316L-IN625 gradient material was prepared by changing the composition ratio of 316L to IN625 along the deposition building direction [Fig. 2(a)]. The powder particles were injected into the molten pool through the 4-path radially symmetric nozzles of the coaxial laser processing head [Fig. 2(b)], and a serpentine scanning trajectory along the short-side direction (SD) was formed. After making the metallographic samples, the microstructural observations were recorded using the BX53M optical microscope (OM) and SU5000 scanning electron microscope (SEM). The phase composition of the different regions was analyzed through the Ultima IV X-ray diffractometer (XRD). In addition, the tensile and microhardness tests were performed using the Z250 universal testing machine and HM-200 Vickers hardness tester, respectively.

Results and Discussions In the 316L region, the segregation of composition occurred at the junction of the grain boundaries, resulting in the generation of irregular inclusions due to the weak bonding force between the inclusions and grain boundaries, where it eventually evolved into microvoids. As the building height increased (70% 316L region), the grain boundaries of cellular dendrites became wider, and the microvoids at the grain boundaries disappeared. Later, epitaxially grown columnar grains were discovered in 40% 316L region. Further, the microstructure transitioned to coarse dendrites, and its primary dendrites spacing decreased (30% 316L region). Finally, the nearly equiaxed grains were formed in the IN625 region, which caused by the faster cooling rate with the alleviation of heat accumulation (Fig. 3). Compared with the joint sample, the 0.2% yield strength of the gradient sample increased with the combination of the high strength IN625. However, the high thermal stress and the possible presence of brittle precipitates (Laves phase) in the gradient regions were prone to causing sample to crack in the early stages of the tensile test, causing a reduction in the tensile strength and the ductility of the gradient sample (Fig. 5). The fracture morphology of the gradient sample showed small holes at the bottom and top of the pits containing the precipitates [Fig. 6(d)]. With the increase of tensile stress, these brittle precipitates separated from the matrix, resulting in brittle dissociation due to uneven plastic deformation. IN625 mainly achieved solid solution strengthening by the refractory metals (Nb and Mo) that were retained in the austenite matrix during the cooling process. Moreover, Nb and Mo located in the previously deposited layer accumulated and eventually precipitated on the matrix as intermetallic phases and carbides under continuous thermal cycling conditions for precipitation strengthening. Due to the combined effect of solid solution and precipitation strengthening, the microhardness of 316L-IN625 gradient material gradually increased with the decrease of the 316L content (Fig. 7).

Conclusions In this work, 316L-IN625 gradient material with the gradient change in the material composition was prepared by LD. The results show that with the reduction of 316L composition, the microstructures of different regions of the gradient material displayed cellular dendrites, columnar grains, coarse dendrites, and nearly equiaxed grains in sequence. Compared with the joint sample, the 0.2% yield strength of the 316L-IN625 gradient sample increased to 289 MPa. However, the tensile strength and the ductility reduced due to the presence of high thermal stress and brittle precipitates. In addition, the tensile deformation mechanisms of joint and gradient samples are ductile cavities and brittle dissociation, respectively. The microhardness of the 316L-IN625 gradient material gradually increases along the deposition building direction, which is related to the solid solution and the precipitation strengthening of IN625.

Key words laser technique; laser deposition; 316L-IN625 gradient material; microstructure; mechanical properties